9-1-2021

Structural insights into the repair mechanism of AGT for methyl-induced DNA damage

Rajendra P. Koirala
Tribhuvan University

Rudramani Pokhrel
Florida International University

Prabin Baral
Florida International University

Purushottam B. Tiwari
Georgetown University

Prem P. Chapagain
Florida International University

See next page for additional authors

Rajendra P. Koirala, Rudramani Pokhrel, Prabin Baral, Purushottam B. Tiwari*, Prem P. Chapagain* and Narayan P. Adhikari*

Structural insights into the repair mechanism of AGT for methyl-induced DNA damage

https://doi.org/10.1515/hsz-2021-0198
Received March 19, 2021; accepted May 29, 2021;
published online June 30, 2021

Abstract: Methylation induced DNA base-pairing damage is one of the major causes of cancer. O^6-alkylguanine-DNA alkyltransferase (AGT) is considered a demethylation agent of the methylated DNA. Structural investigations with thermodynamic properties of the AGT-DNA complex are still lacking. In this report, we modeled two catalytic states of AGT-DNA interactions and an AGT-DNA covalent complex and explored structural features using molecular dynamics (MD) simulations. We utilized the umbrella sampling method to investigate the changes in the free energy of the interactions in two different AGT-DNA catalytic states, one with methylated GUA in DNA and the other with methylated CYS145 in AGT. These non-covalent complexes represent the pre- and post-repair complexes. Therefore, our study encompasses the process of recognition, complex formation, and separation of the AGT and the damaged (methylated) DNA base. We believe that the use of parameters for the amino acid and nucleotide modifications and for the protein-DNA covalent bond will allow investigations of the DNA repair mechanism as well as the exploration of cancer therapeutics targeting the AGT-DNA complexes at various functional states as well as explorations via stabilization of the complex.

***Corresponding authors: Purushottam B. Tiwari**, Department of Oncology, Georgetown University, Washington, D.C., USA, E-mail: pbt7@georgetown.edu. https://orcid.org/0000-0002-3140-0723; **Prem P. Chapagain**, Department of Physics, Florida International University, Miami, FL, USA; and Biomolecular Sciences Institute, Florida International University, Miami, FL, USA, E-mail: chapagap@fiu.edu. https://orcid.org/0000-0002-0999-4975; and **Narayan P. Adhikari**, Central Department of Physics, Tribhuvan University, Kathmandu, Nepal, E-mail: narayan.adhikari@cdp.tu.edu.np. https://orcid.org/0000-0003-4535-1368
Rajendra P. Koirala, Central Department of Physics, Tribhuvan University, Kathmandu, Nepal, E-mail: rajendra.koirala@cdp.tu.edu.np
Rudramani Pokhrel and Prabin Baral, Department of Physics, Florida International University, Miami, FL, USA, E-mail: rpokh002@fiu.edu (R. Pokhrel), pbara006@fiu.edu (P. Baral)

Keywords: AGT-DNA complex; DNA methylation; DNA repair; MD simulations; umbrella sampling.

Introduction

DNA base-pairing damage involves chemical modifications such as base mismatch and methylation of DNA bases (Crone et al. 1996; Kyrtopoulos et al. 1997; Maser and DePinho, 2002) and is one of the major causes of cancer (Jackson and Bartek 2009; Paulsen and Ferguson-Smith 2001). Methylation of a DNA base can cause carcinogenesis of a living cell (De Bont and van Larebeke 2004; Lindahl and Barnes 2000; Tessmer and Fried 2014; Warren et al. 2006). O^6-alkylguanine-DNA alkyltransferase (AGT) functions as the demethylation agent for the O^6-alkylguanine and O^4-alkylthymine DNA bases (Gerson 2002; Harris et al. 1992; Kelley and Fishel 2008; McKeague et al. 2018; Zak et al. 1994). The interaction of AGT with DNA is considered as a novel interaction mechanism for the recognition of DNA damage and repair (Daniels et al. 2004; Musarrat et al. 1995; Perugino et al. 2012; Rossi et al. 2018). After locating the DNA damage, AGT accesses the alkylated base by flipping the nucleotide into the protein so that the methylated GUA approaches the enzyme active site. Once the methylated GUA is in the active site, it donates its methyl group to the CYS145 residue in AGT (Ali et al. 1998; Duguid et al. 2005).

Because it confers protection against DNA damage, AGT plays a crucial role to protect normal cells from tumorigenesis. For example, it is shown to protect against methylation-induced skin cancer (Becker et al. 1996), liver cancer (Nakatsuru et al. 1993), lung cancer (Liu et al. 1999; Sakumi et al. 1997), and thymic lymphomas (Dumenco et al. 1993). However, AGT can also provide undesired protection to cancer cells from damage due to methylating and chloroethylating anticancer drugs (Fu et al. 2012; Kaina et al. 2007; Rasimas et al. 2003), thus fostering drug resistance. Therefore, AGT is an important drug target for improving the efficacy of chemotherapy.

Despite previous investigations of this functionally important DNA-AGT complex, structural investigations with thermodynamic properties of the complex are still lacking. Computational investigations of the demethylation process

of methylated DNA bases by AGT are limited due to the lack of pre-defined force-field parameters. In this work, we utilized computational approaches with CHARMM36m (Huang et al. 2017) force field parameters to create covalent and non-covalent complexes and explored their suitability to investigate structural features of the complex using molecular dynamics (MD) simulations. Such structural investigations have increasingly been used in recent years for investigating complexes of proteins with other partners (Magnen et al. 2018; Tiwari et al. 2016, 2018, 2020), including the protein-DNA covalent complex with implications in drug discovery (Tiwari et al. 2020). We used the umbrella sampling method to calculate the changes in the free energies in AGT-DNA complexes in two non-covalent complexes in different states of methylation, pre- and post-repair structures, one with methylated GUA in DNA and the other with methylated CYS145 in AGT. This technique allows the determination of energetically favorable states and has been used in studies of many bio-molecular systems (Luzhkov 2017; Pokhrel et al. 2019). The use of the parameters for the amino acid and nucleotide modifications and for the protein-DNA covalent bond allows computational investigations of the AGT-DNA complex structures before and after methyl transfer, as well as the AGT-DNA covalent complex. Such investigations will be useful for future explorations of cancer therapeutics targeting the AGT-DNA complexes at various functional states as well as explorations via stabilization of the complex. For example, the catalytic site in the transient state of the DNA-AGT complex may provide a novel target for in silico drug screening to identify AGT inhibitors that inhibit the methyl transfer, potentially overcoming the anticancer drug resistance to improve the efficacy of chemotherapy.

Results

Dynamics of the AGT-DNA covalent and non-covalent complexes

We generated all three complexes – complex-I, complex-II, and complex-III as explained in the Methods section. The complex-I has methylated GUA7 (6OG7) in DNA, complex-II represents a possible model of a transient, intermediate state in which methylated GUA7 covalently bonded to CYS145, and complex-III has methylated CYS (ORT145) in AGT. In the complex-I, GUA7 is methylated at O^6 point and this methyl group is supposed to be transferred to CYS145 in AGT whereas the methyl group in GUA7 is transferred to CYS145 in complex-III. In this transfer, the sulfur atom of CYS145 side chain becomes deprotonated and the methyl group gets attached to it. Figure 1A shows a representative AGT-DNA complex (complex-I). Figure 1B displays the covalent bonding between the 6OG7 and CYS145. It is to be noted that in the AGT-DNA covalent complex in the protein data bank (PDB ID 1T39), CYS145 is cross-linked to the mechanistic inhibitor N^1, O^6-ethanoxanthosine (Daniels et al. 2004) as shown in Figure 1C. This inhibitor was purposely used to prevent the methyl transfer and achieve a stable covalent complex, resulting in the covalent bonding seen in Figure 1C in contrast to Figure 1B, which represents the transient, intermediate catalytic state during the methyl transfer process. Figure 1D shows the pre-catalytic state with methylated GUA7 (6OG7) and Figure 1E shows the post-catalytic state with methylated CYS145, both without a covalent bond between the GUA and CYS. The CYS145 residue (with or without the hydrogen attached to the sulfur) is enclosed within a circle in Figure 1B–E.

We performed 200 ns of MD simulations for each of the three complexes to ensure the stability of the complexes and to investigate structural dynamics. A representative simulation movie of the 200 ns CPT production run for the AGT-DNA covalent complex, complex-II, is given in the Supplementary Material (Section S3). The DNA appears to be flexible at the ends, especially at the lower end. We calculated the total interaction energies using the 200 ns simulation trajectories of each of the three complexes and results are shown in Figure 2A. There is no significant fluctuation in the total energy for all three systems, suggesting the stability of the complexes (Tiwari et al. 2018). Figure 2B also shows that there was no significant fluctuation in RMSD in all the three complexes. The total number of hydrogen bonds formed between AGT and DNA as a function of simulation time shows a similar level of hydrogen bonding in all three complexes (Figure 2C). A detailed analysis of the AGT-DNA hydrogen bonding shows that residues TYR114 and CYS145 (or ORT145) in AGT consistently form hydrogen bonding with 6OG7 (or GUA7). These residues and nucleotides may be important in the formation of the complexes. Table 1 shows all residues in AGT and nucleotides in DNA that establish hydrogen bonding with occupancy greater than 40%. We have also calculated hydrogen-bonding distances for the two residue-nucleotide pairs and presented in Figure 2D–F, for complex-I, complex-II, and complex-III, respectively. As expected the weaker hydrogen bonding was observed for the complex-III (post-catalytic state) as compared to complex-I (pre-catalytic state) as can be seen in Figure 2D, F as well as in Table 1. Even though TYR114-GUA7 in the complex-III bonding looks as stable as TYR114-6OG7 in the complex-I, the occupancy of this hydrogen bonding is much less (~59%) in the complex-III as compared to the

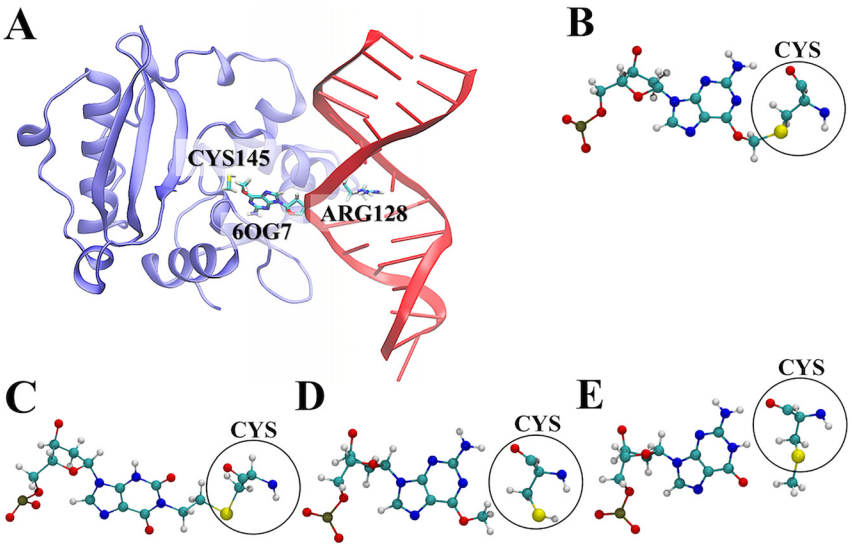

Figure 1: (A) A representative structure of the AGT-DNA complex (Complex I). The intercalating residue ARG128 in AGT, O^6-methylguanine (6OG7) in DNA, and nearby CYS145 in AGT are shown in stick representations. (B) Covalent bonding between AGT and DNA at the biological substrate O^6-methylguanine (6OG7). (C) Covalent bonding between AGT and DNA cross-linked to the mechanistic inhibitor N^1, O^6-ethanoxanthosine as presented in the PDB ID 1T39 (Daniels et al. 2004). (D) CYS145 in AGT and 6OG7 in DNA without the covalent bonding. (E) Methylated CYS145 (ORT145) in AGT and GUA7 in DNA without the covalent bonding. The AGT residues and DNA nucleotides forming the covalent bonding in Figure 1A and the residues and nucleotides in Figure 1B–E are shown in colored CPK representation. The CYS145 portions (with or without hydrogen atom bound to the sulfur atom) in Figure 1B–E are enclosed within circles.

complex-I (~88%). We believe that the stronger hydrogen bonding in the complex-I corresponds to the recognition of DNA by AGT for the methyl transfer process. We also observed that three water molecules reside within interfacial region between AGT and DNA during the 200 ns simulation of the complex-I and form two water-mediated hydrogen bonds between ARG128 and CYT8, and one between LYS125 and CYT21, as shown in Figure S1 (Supplementary Material

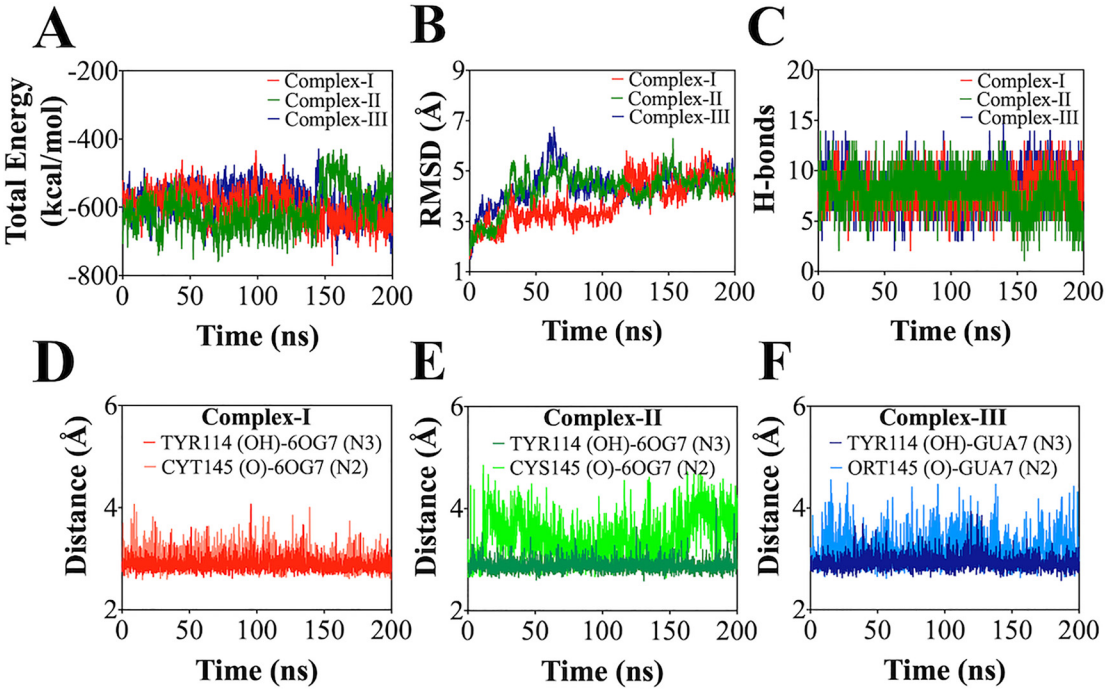

Figure 2: (A) Total energy, (B) RMSD measurements, (C) number of hydrogen bonds between AGT and DNA, and (D)–(F) distances between atoms in residues and nucleotides forming hydrogen bonds in the three AGT-DNA complexes (complex-I, complex-II, and complex-III) calculated using 200 ns simulation trajectories.

Table 1: AGT residues and DNA nucleotides establishing hydrogen bonding between AGT and DNA with occupancy greater than 40%.

AGT-DNA complex	Residue-nucleotide pairs		Occupancy
	AGT	DNA	
Complex-I	TYR114 (OH)	6OG7 (N3)	87.6%
	CYS145 (O)	6OG7 (N2)	87.1%
	SER151 (OG)	THY9 (O1P)	85.6%
	THR95 (OG1)	THY23 (O1P)	80.3%
	SER151 (N)	THY9 (O2P)	69.6%
	THR95 (N)	THY23 (O1P)	62.8%
	GLN115 (N)	THY9 (O1P)	53.2%
Complex-II	SER151 (OG)	THY9 (O1P)	90.0%
	TYR114 (OH)	6OG7 (N3)	71.6%
	THR95 (OG1)	THY23 (O1P)	69.2%
	SER151 (N)	THY9 (O2P)	68.4%
	THR95 (N)	THY23 (O1P)	56.1%
	CYS145 (O)	6OG7 (N2)	53.8%
	GLN115 (N)	THY9 (O1P)	48.9%
	ARG128 (NH2)	CYT20 (N3)	47.8%
Complex-III	TYR114 (OH)	GUA7 (N3)	59.0%
	SER151 (N)	THY9 (O1P)	55.8%
	PHE94 (N)	THY23 (O1P)	48.4%
	ORT145 (O)	GUA7 (N1)	47.8%
	ARG135 (NH1)	GUA7 (O5′)	44.6%
	ASN157 (ND2)	GUA7 (O4′)	43.7%
	ORT145 (O)	GUA7 (N2)	40.9%

The atoms that are predicted by VMD to be responsible for establishing the hydrogen bondings are presented inside parentheses.

Section S4). While we did not observe these water-mediated hydrogen bonding in complexes II and III during the simulated timescales, such water occupancy may occur in longer timescales.

DNA-AGT complex formation and dissociation

To investigate the underlying mechanism of AGT-DNA complex formation (pre-catalytic, formation of complex-I) and dissociation (post-catalytic, complex-III) process, we performed umbrella sampling for different separation distances between AGT and DNA. For this, DNA was translated, along the negative *x*-axis, relative to AGT by 1 Å window for 19 windows. The direction of the displacement was chosen visually based on the orientation of the intercalated ARG128 side-chain as well as the flipped GUA7 base so that when displaced, they are minimally obstructed by other residues (i.e. nearly parallel to the ARG128 sidechain and the flipped base and directly away from AGT). The complex was then re-oriented so that the direction of the displacement lies along the *x*-axis for convenience. Figure S2A in the Supplementary Material (Section S5) depicts the direction of translation. Two sets of these windows were prepared, one with methylated GUA7 (6OG7) and the other with methylated CYS145 (ORT145). The access of AGT to the alkylated base only occurs when alkylated based is flipped out of the base stack and into the AGT active site for extrahelical repair and ARG128 facilitates the base flipping (Daniels et al. 2004). As the base flipping is observed to occur at a rate of $k = 350\ s^{-1}$ (Zang et al. 2005) (i.e. in the order of milliseconds), base flipping and the associated conformational transitions upon AGT binding are not accessible in our simulated timescales. Therefore, we used the pre-catalytic complex as our starting structure, which is formed when the methylated GUA base is flipped and captured into the AGT active site. Once the complex is formed and the methyl is transferred to CYS145, the repaired DNA undergoes slow dissociation from AGT (Zang et al. 2005). It is also observed that post-transfer methylated AGT can remain bound to DNA and undergoes ubiquitination and degradation (Tessmer et al. 2012). The set with the methylated CYS145 represents the process during the dissociation of the complex. We calculated the non-bonded interaction energies as a function of the separation distance (COM distance) for both of these processes. Figure 3 shows the contribution of van der Waals and electrostatic energies averaged over 10 ns simulations at various COM distances. As shown in Figure 3A (complex-I) and Figure 3B (complex-III), the electrostatic energy was found to have the major contribution to the interaction energies. A modest contribution from the van der Waals interaction is observed for COM distance <32.8 Å as the methylated GUA7 approaches the active site (Figure 3A) or GUA7 separates from the active site (Figure 3B). The Representative snapshots of the complex-I at different COM distances are shown in the Supplementary Material (Figure S2, Section S5). When the distance is gradually increased from 32.8 Å, AGT dissociates from the minor groove of DNA, losing the original AGT-DNA interactions and forming new interactions. The intercalating residue ARG128 interacts strongly with GUA7 when the COM distance >37 Å. The RMSD measurements (shown in Figure S3, Section S6) are fairly stable in each of the 10 ns windows, indicating the convergence of simulations.

To understand the energetic differences in the approach of the damaged base versus separation of the repaired base, we calculated the free energies for these processes using umbrella sampling along the COM as the reaction coordinate. While COM is a good order parameter for comparing the stability of the protein-DNA complex, we note that the distance between the sulfur atom of CYS145 and the oxygen atom of the GUA7 base (S-O distance) can also be chosen as a reaction coordinate. Figure 4 shows the change in free energy for approaching

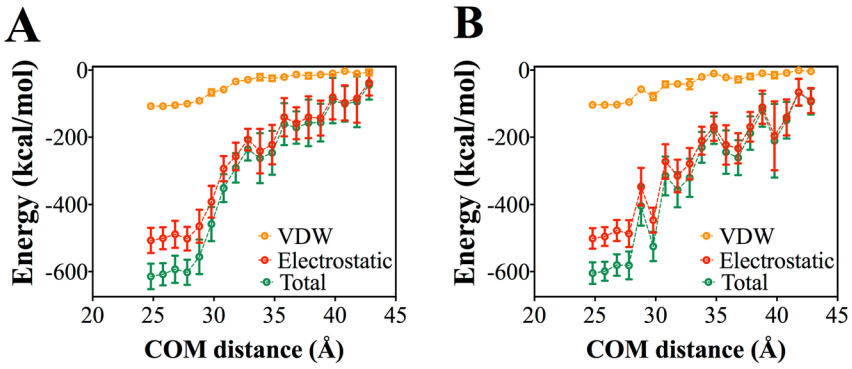

Figure 3: Variation of non-bonded interaction energies with the displacement of DNA from AGT.
Van der Waal interaction energy (VDW, orange color), electrostatic interaction energy (E, red color) and total non-bonded energy (E+VDW, green color) was calculated using NAMD energy plugin within VMD for complex-I (A) and for complex-III (B). Symbols and error bars represent average and standard deviation, respectively, calculated from the 10 ns NAMD simulation trajectories for the complexes at each COM distance. Dotted lines are guides to eyes.

methylated GUA7 to the active site (complex-I) as well as for separating demethylated GUA7 from the active site (complex-III). To compare the free-energies of the complexes with GUA7 at the active site, we aligned the curves when the DNA and AGT are fully separated, at which point the free energies for both systems should be comparable as the interaction between DNA and AGT is negligible for the COM distance >42 Å, after 18th window. As shown in Figure 4, the change in free energy for the complex-I, ΔG_1, between the complexed and separated states was found to be ~11.1 kcal/mol and that for the complex-III, ΔG_2, was ~9.8 kcal/mol. Comparison of the lowest free energy values at ~26 Å COM distance, which represents the state in which the GUA7 or 6OG7 in the catalytic cavity, shows that the pre-transfer 6OG7 is more favorable in the cavity compared to the post-transfer GUA7, giving a free-energy advantage for 6OG7 of $\Delta\Delta G \sim -1.3$ kcal/mol over GUA7. This may facilitate the dissociation of the GUA7 from the cavity once the methyl group is transferred to CYS145. Also, the shallower free energy curve beyond ~28 Å for complex-III indicates an easier dislodgement of the post-transfer GUA7. These observations explain the affinity of 6OG7 over GUA7 in the catalytic cavity, giving an insight into the base demethylation mechanism of AGT.

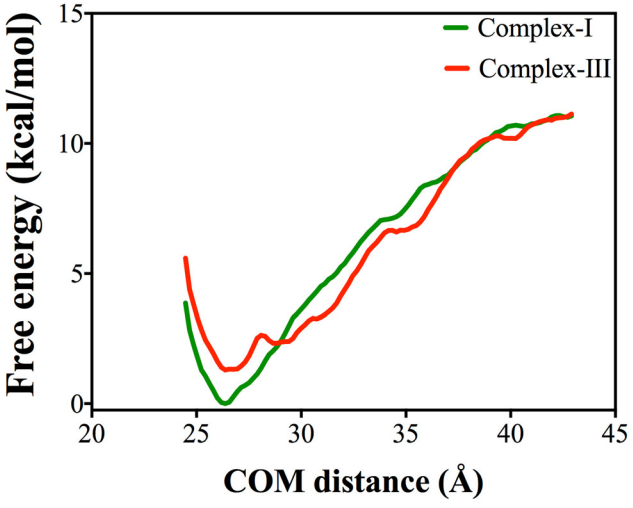

Figure 4: Change in free energy for complex-I and complex-III as a function of COM distance.

Discussion

AGT is considered as the demethylation agent to repair the methyl-damaged DNA (Hu et al. 2008; Tessmer and Fried 2014; Tubbs et al. 2007). The entry of AGT near the damaged part of DNA is the fundamental requirement to initiate the methyl transfer process (McKeague et al. 2018) by forming a transient complex between the two molecules (Daniels et al. 2004; Duguid et al. 2005; Fang et al. 2008). Methylation of a DNA base is one of the major causes of the carcinogenesis of a living cell (Lindahl and Barnes 2000; Tessmer and Fried 2014). While AGT plays a crucial role in repairing the DNA damage and protect the normal cells from tumor development, it can also allow anticancer drug resistance by protecting the cancer cells from anticancer drugs (Kaina et al. 2007; Rasimas et al. 2003; Fu et al. 2012) that aim at damaging the DNA. Given its importance as a drug target for overcoming anticancer drug resistance to improve chemotherapeutic efficacy, structural models of the AGT-DNA complex in different functional states of the methyl transfer process are desired for biophysical insights as well as for in silico screening. For example, small molecules interfering the covalent complex formation and release can potentially inhibit the DNA repair process, improving the efficacies of the anticancer drugs given in combination. Motivated by this, we have created the covalent complex between AGT and DNA and performed subsequent MD simulations to investigate its structural features and we believe that the complex-II

generated in this work with the force field modifications may be useful in the structure-based discovery of anticancer agents. We note that our transient intermediate model uses the covalently linked sp^3 hybridized carbon between S and O (i.e. –S ··· CH_2 ··· O–). However, the actual transfer of methyl group to sulfur from methylguanine is considered to occur via a S_N2-like mechanism (Daniels et al. 2000; Mattossovich et al. 2020), which involves a planar, penta-coordinated carbon (–S ··· CH_3 ··· O–) (Fernández et al. 2007) as the transient intermediate with short lifetime (Fu et al. 2021). While the orientations of the groups and the nature of the cavity that likely occur in the order of 100 ns timescales (Patra et al. 2016) may be sufficiently represented by our model for the purpose of stabilizing the complex, further work with appropriate force-field modifications for penta-coordinate carbon is needed for a more detailed analysis of the geometry and energetics of the transition state.

To gain insights into the DNA repair mechanism of AGT, we performed umbrella sampling and calculated free energy and presented results in Figure 4 from 10 ns simulations. We also performed the sampling with 20 ns up to COM distance of 40 Å for Complex-I and we did not see much change compared to the 10 ns sampling. This comparison is shown in the Supplementary Material (Figure S4, Section S7). Figure 4 shows the free energy as a function of separation distance between AGT and DNA for both systems – with methylated GUA and with methylated CYS, representing the pre- and post-transfer of the methyl group. In actual post-transfer process, slight displacement of the AGT helix 6 in the helix-turn-helix motif resulting from the steric hindrance due to methylation of CYS145 may facilitate the release of the repaired DNA from the cavity, and subsequent ubiquitination and protein degradation (Daniels et al. 2000). In our simulations, only a slight increase in RMSD is observed (Figure 2B) in complex III (post-transfer) compared to complex I (pre-transfer) and the process of conformational changes resulting in the repaired base release is difficult to obtain in our computational timescales. Here, the post-transfer separation of DNA-AGT was studied with manual translation of DNA relative to AGT with an increment of 1 Å displacement along the negative x-direction.

The COM distance as a reaction coordinate allows us to track the free-energy changes for both of these processes and compare the differences in the affinity for the methylated versus demethylated GUA in the catalytic cavity. The interaction energies (shown in Figure 2A) were not able to clearly differentiate the structural changes, which is understandable but the free-energy calculations, more relevant to the binding assays, do show the difference between pre- and post-transfer. The methylated GUA is found to have an affinity of $\Delta\Delta G \sim -1.3$ kcal/mol in the cavity compared to the unmethylated GUA after the methyl group is transferred. This, as well as the nature of the free-energy curve, provides an insight into the base demethylation mechanism of AGT. Finally, our study encompasses the pre-transfer, model intermediate and post-transfer complexes, and separation of the AGT and the damaged (methylated) DNA base and provides models for computational investigations of the DNA repair mechanism as well as for the exploration of cancer therapeutics targeting these AGT-DNA complexes at various functional states.

Materials and methods

System setup

The molecular structures, PDB IDs 1T38 and 1T39 (Daniels et al. 2004), were taken from the protein data bank to create the input structures for MD simulations. The PDB structure 1T38 contains the protein-DNA non-covalent complex with a methyl group attached to the O^6-position of GUA7 (named as 6OG7) of the DNA (complex-I). The PDB structure 1T39 contains the protein-DNA covalent-complex (complex-II). CHARMM-GUI (Lee et al. 2016) was used to fulfill the missing residues in both PDB structures. We used VMD (Humphrey et al. 1996) to create the non-covalent AGT-DNA system with methylated GUA7 (complex-I) with CHARMM36m (Huang et al. 2017) force-field. The residue SER145 in the PDB ID 1T38 was replaced with CYS. The GUA methylation required additional force field parameters, which are given in Supplementary Material (Section S1). Similarly, for generating the AGT-DNA covalent system (complex-II), we first converted the residue E1X7 in the PDB ID 1T39 to methylated GUA7 and then applied a patch to connect the methylated GUA7 and CYS145, resulting in a covalent bond between the protein and DNA. Finally, the non-covalent AGT-DNA system with methylated CYS145 (complex-III) was set up using the PDB ID 1T38 with additional set of force-field parameters for CYS methylation. The additional topology and parameters used to generate all the three complexes are given in Supplementary Material (Sections S1 and S2). Each of these complexes was solvated with TIP3P water in cubic box and electrically neutralized by adding NaCl. The non-covalent complexes-I and -III used in the umbrella sampling simulations were solvated in orthorhombic boxes.

Molecular dynamics simulation

All-atom molecular dynamics (MD) simulations were performed using the NAMD simulation package (Phillips et al. 2005). The CHARMM36m (Huang et al. 2017) force field was used in simulations of all the complex structures. The additional force field parameters that were used to simulate the three different complexes are given in the Supplementary Material (Section S2). The Particle Mesh Edward (PME) was used for the long-range interactions with a 12.0 Å non-bonded cutoff.

The energy minimization was performed for 10,000 steps, using the conjugate gradient and line search algorithm. Each system was then equilibrated with harmonically restrained heavy atoms at 300 K using 1 fs time step. The production runs were performed using Langevin dynamics with a damping constant of 1 ps^{-1} under CPT conditions.

Umbrella sampling

Umbrella sampling was performed for the complex-I and complex-III systems. We prepared 19 different 1 Å windows for each system with the AGT protein taken as a reference molecule and DNA was translated along the negative x-direction by manual displacement. The window size ensures the sufficient overlapping of successive windows to cover the entire reaction coordinate space (Banavali and MacKerell 2002; Luzhkov 2017; Sugita et al. 2000). The reaction coordinate was chosen as the distance between the center-of-mass (COM) of AGT and DNA along the negative x-axis. To make the necessary overlapping reaction coordinates, a bias potential $V(x)$ was used to force the system to fluctuate in coordinate space, which is given by, $V(x) = \frac{1}{2}k_i(x - x_0)^2$, where x_0 is the harmonic constraint defining a center of window i (i = 1 to 19), and force constant k_i is the window width. Although the harmonic potential fluctuates the system to overlap the reaction coordinates, the windows are still unbiased. We used the force constant of 1.5 kcal mol^{-1} $Å^{-2}$.

Data analysis

VMD (Humphrey et al. 1996) was used to analyze the simulation trajectories and visualize the structures. The NAMD energy plugin, available in VMD was used to calculate the non-bonded interaction energies; electrostatics (E), van der Waals (VDW) contributions. The potential energy contributions to electrostatic and VDW energy are given by $U_E = \frac{q_1 q_2}{4\pi\epsilon_0 r}$ and $U_{VDW} = 4\epsilon\left[\left(\frac{\sigma}{r}\right)^{12} - \left(\frac{\sigma}{r}\right)^{6}\right]$, respectively (Phillips et al. 2005), where q_1 and q_2 are charges of the interacting pairs separated at a distance r, ϵ_0 is the permittivity of the free space, ϵ is the depth of the potential well, and σ is the distance at which the potential energy is zero. VMD was used to analyze hydrogen bonding between AGT residues and DNA nucleotides. The free energy was estimated by the Weighted Histogram Analysis Method (WHAM) (Kumar et al. 1992) program. GaphPad prism (San Diego, CA) was used to plot the graphs.

Acknowledgments: We sincerely thank Professor Alexander D. MacKerell Jr. at the Computer-Aided Drug Design Center, University of Maryland, USA, for his valuable input and help with the force-field parameters. R.P.K. acknowledges the partial financial support from the Nepal Academy of Science and Technology (NAST). N.P.A. acknowledges the UGC Award No. CRG-73/74-S&T-01 and Associate membership of The Abdus Salam International Center for Theoretical Physics, Trieste, Italy.

Author contributions: P.B.T., P.P.C., and N.P.A. guided the project. R.P.K, R.P., P.B., and P.B.T performed MD simulations. R.P.K., R.P., P.B., P.B.T., P.P.C., and N.P.A. analyzed the data. R.P.K., P.B.T., and P.P.C. wrote the manuscript. R.P., P.B., and N.P.A. contributed to the manuscript editing.

Research funding: This work was supported by University Grants Commission- Nepal (CRG-73/74-S&T-01).

Conflict of interest statement: The authors declare no conflict of interest.

References

Ali, R.B., Teo, A.K., Oh, H.K., Chuang, L.S., Ayi, T.C., and Li, B.F. (1998). Implication of localization of human DNA repair enzyme O^6-methylguanine-DNA methyltransferase at active transcription sites in transcription-repair coupling of the mutagenic O^6-methylguanine lesion. Mol. Cell. Biol. 18: 1660–1669.

Banavali, N.K. and MacKerell, A.D., Jr. (2002). Free energy and structural pathways of base flipping in a DNA GCGC containing sequence. J. Mol. Biol. 319: 141–160.

Becker, K., Dosch, J., Gregel, C.M., Martin, B.A., and Kaina, B. (1996). Targeted expression of human O(6)-methylguanine-DNA methyltransferase (MGMT) in transgenic mice protects against tumor initiation in two-stage skin carcinogenesis. Canc. Res. 56: 3244–3249.

Crone, T.M., Goodtzova, K., and Pegg, A.E. (1996). Amino acid residues affecting the activity and stability of human O^6-alkylguanine-DNA alkyltransferase. Mutat. Res. 363: 15–25.

Daniels, D.S., Mol, C.D., Arvai, A.S., Kanugula, S., Pegg, A.E., and Tainer, J.A. (2000). Active and alkylated human AGT structures: a novel zinc site, inhibitor and extrahelical base binding. EMBO J. 19: 1719–1730.

Daniels, D.S., Woo, T.T., Luu, K.X., Noll, D.M., Clarke, N.D., Pegg, A.E., and Tainer, J.A. (2004). DNA binding and nucleotide flipping by the human DNA repair protein AGT. Nat. Struct. Mol. Biol. 11: 714–720.

De Bont, R. and van Larebeke, N. (2004). Endogenous DNA damage in humans: a review of quantitative data. Mutagenesis 19: 169–185.

Duguid, E.M., Rice, P.A., and He, C. (2005). The structure of the human AGT protein bound to DNA and its implications for damage detection. J. Mol. Biol. 350: 657–666.

Dumenco, L.L., Allay, E., Norton, K., and Gerson, S.L. (1993). The prevention of thymic lymphomas in transgenic mice by human O^6-alkylguanine-DNA alkyltransferase. Science 259: 219–222.

Fang, Q., Noronha, A.M., Murphy, S.P., Wilds, C.J., Tubbs, J.L., Tainer, J.A., Chowdhury, G., Guengerich, F.P., and Pegg, A.E. (2008). Repair of O^6-G-alkyl-O^6-G interstrand cross-links by human O^6-alkylguanine-DNA alkyltransferase. Biochemistry 47: 10892–10903.

Fernández, I., Uggerud, E., and Frenking, G. (2007). Stable pentacoordinate carbocations: structure and bonding. Chemistry 13: 8620–8626.

Fu, D., Calvo, J.A., and Samson, L.D. (2012). Balancing repair and tolerance of DNA damage caused by alkylating agents. Nat. Rev. Canc. 12: 104–120.

Fu, Y., Bernasconi, L., and Lu, P. (2021). Ab initio molecular dynamics simulations of the S_N1/S_N2 mechanistic continuum in glycosylation reactions. J. Am. Chem. Soc. 143: 1577–1589.

Gerson, S.L. (2002). Clinical relevance of MGMT in the treatment of cancer. J. Clin. Oncol. 20: 2388–2399.

Harris, L.C., Potter, P.M., and Margison, G.P. (1992). Site directed mutagenesis of two cysteine residues in the E. coli OGT O^6-alkylguanine DNA alkyltransferase protein. Biochem. Biophys. Res. Commun. 187: 425–431.

Hu, J., Ma, A., and Dinner, A.R. (2008). A two-step nucleotide-flipping mechanism enables kinetic discrimination of DNA lesions by AGT. Proc. Natl. Acad. Sci. U. S. A. 105: 4615–4620.

Huang, J., Rauscher, S., Nawrocki, G., Ran, T., Feig, M., de Groot, B.L., Grubmüller, H., and MacKerell, A.D. (2017). CHARMM36m: an improved force field for folded and intrinsically disordered proteins. Nat. Methods 14: 71–73.

Humphrey, W., Dalke, A., and Schulten, K. (1996). VMD: visual molecular dynamics. J. Mol. Graph. 14: 27–28.

Jackson, S.P. and Bartek, J. (2009). The DNA-damage response in human biology and disease. Nature 461: 1071–1078.

Kaina, B., Christmann, M., Naumann, S., and Roos, W.P. (2007). MGMT: key node in the battle against genotoxicity, carcinogenicity and apoptosis induced by alkylating agents. DNA Repair 6: 1079–1099.

Kelley, M.R. and Fishel, M.L. (2008). DNA repair proteins as molecular targets for cancer therapeutics. Anti Canc. Agents Med. Chem. 8: 417–425.

Kumar, S., Rosenberg, J.M., Bouzida, D., Swendsen, R.H., and Kollman, P.A. (1992). The weighted histogram analysis method for free-energy calculations on biomolecules. I. The method. J. Comput. Chem. 13: 1011–1021.

Kyrtopoulos, S.A., Anderson, L.M., Chhabra, S.K., Souliotis, V.L., Pletsa, V., Valavanis, C., and Georgiadis, P. (1997). DNA adducts and the mechanism of carcinogenesis and cytotoxicity of methylating agents of environmental and clinical significance. Canc. Detect. Prev. 21: 391–405.

Lee, J., Cheng, X., Swails, J.M., Yeom, M.S., Eastman, P.K., Lemkul, J.A., Wei, S., Buckner, J., Jeong, J.C., Qi, Y., et al. (2016). CHARMM-GUI input generator for NAMD, GROMACS, AMBER, OpenMM, and CHARMM/OpenMM simulations using the CHARMM36 additive force field. J. Chem. Theor. Comput. 12: 405–413.

Lindahl, T. and Barnes, D.E. (2000). Repair of endogenous DNA damage. Cold Spring Harbor Symp. Quant. Biol. 65: 127–133.

Liu, L., Qin, X., and Gerson, S.L. (1999). Reduced lung tumorigenesis in human methylguanine DNA–methyltransferase transgenic mice achieved by expression of transgene within the target cell. Carcinogenesis 20: 279–284.

Luzhkov, V.B. (2017). Molecular modelling and free-energy calculations of protein—ligand binding. Russ. Chem. Rev. 86: 211.

Magnen, M., Elsasser, B.M., Zbodakova, O., Kasparek, P., Gueugnon, F., Petit-Courty, A., Sedlacek, R., Goettig, P., and Courty, Y. (2018). Kallikrein-related peptidase 5 and seasonal influenza viruses, limitations of the experimental models for activating proteases. Biol. Chem. 399: 1053–1064.

Maser, R.S. and DePinho, R.A. (2002). Connecting chromosomes, crisis, and cancer. Science 297: 565–569.

Mattossovich, R., Merlo, R., Miggiano, R., Valenti, A., and Perugino, G. (2020). O^6-alkylguanine-DNA alkyltransferases in microbes living on the edge: from stability to applicability. Int. J. Mol. Sci. 21: 2878.

McKeague, M., Otto, C., Raz, M.H., Angelov, T., and Sturla, S.J. (2018). The base pairing partner modulates alkylguanine alkyltransferase. ACS Chem. Biol. 13: 2534–2541.

Musarrat, J., Wilson, J.A., Abouissa, H., and Wani, A.A. (1995). O^6-alkylguanine DNA alkyltransferase activity levels in normal, benign and malignant human female breast. Biochem. Biophys. Res. Commun. 208: 688–696.

Nakatsuru, Y., Matsukuma, S., Nemoto, N., Sugano, H., Sekiguchi, M., and Ishikawa, T. (1993). O^6-methylguanine-DNA methyltransferase protects against nitrosamine-induced hepatocarcinogenesis. Proc. Natl. Acad. Sci. U. S. A. 90: 6468–6472.

Patra, N., Ioannidis, E.I., and Kulik, H.J. (2016). Computational investigation of the interplay of substrate positioning and reactivity in catechol O-methyltransferase. PloS One 11: e0161868.8.

Paulsen, M. and Ferguson-Smith, A.C. (2001). DNA methylation in genomic imprinting, development, and disease. J. Pathol. 195: 97–110.

Perugino, G., Vettone, A., Illiano, G., Valenti, A., Ferrara, M.C., Rossi, M., and Ciaramella, M. (2012). Activity and regulation of archaeal DNA alkyltransferase: conserved protein involved in repair of DNA alkylation damage. J. Biol. Chem. 287: 4222–4231.

Phillips, J.C., Braun, R., Wang, W., Gumbart, J., Tajkhorshid, E., Villa, E., Chipot, C., Skeel, R.D., Kale, L., and Schulten, K. (2005). Scalable molecular dynamics with NAMD. J. Comput. Chem. 26: 1781–1802.

Pokhrel, R., Pavadai, E., Gerstman, B.S., and Chapagain, P.P. (2019). Membrane pore formation and ion selectivity of the Ebola virus delta peptide. Phys. Chem. Chem. Phys. 21: 5578–5585.

Rasimas, J.J., Pegg, A.E., and Fried, M.G. (2003). DNA-binding mechanism of O^6-alkylguanine-DNA alkyltransferase. Effects of protein and DNA alkylation on complex stability. J. Biol. Chem. 278: 7973–7980.

Rossi, F., Morrone, C., Massarotti, A., Ferraris, D.M., Valenti, A., Perugino, G., and Miggiano, R. (2018). Crystal structure of a thermophilic O^6-alkylguanine-DNA alkyltransferase-derived self-labeling protein-tag in covalent complex with a fluorescent probe. Biochem. Biophys. Res. Commun. 500: 698–703.

Sakumi, K., Shiraishi, A., Shimizu, S., Tsuzuki, T., Ishikawa, T., and Sekiguchi, M. (1997). Methylnitrosourea-induced tumorigenesis in MGMT gene knockout mice. Canc. Res. 57: 2415–2418.

Sugita, Y., Kitao, A., and Okamoto, Y. (2000). Multidimensional replica-exchange method for free-energy calculations. J. Chem. Phys. 113: 6042–6051.

Tessmer, I. and Fried, M.G. (2014). Insight into the cooperative DNA binding of the O(6)-alkylguanine DNA alkyltransferase. DNA Repair 20: 14–22.

Tessmer, I., Melikishvili, M., and Fried, M.G. (2012). Cooperative cluster formation, DNA bending and base-flipping by O^6-alkylguanine-DNA alkyltransferase. Nucleic Acids Res. 40: 8296–8308.

Tiwari, P.B., Chapagain, P.P., Banda, S., Darici, Y., Üren, A., and Tse-Dinh, Y.-C. (2016). Characterization of molecular interactions between Escherichia coli RNA polymerase and topoisomerase I by molecular simulations. FEBS Lett. 590: 2844–2851.

Tiwari, P.B., Chapagain, P.P., Seddek, A., Annamalai, T., Üren, A., and Tse-Dinh, Y.-C. (2020). Covalent complex of DNA and bacterial topoisomerase: implications in antibacterial drug development. ChemMedChem 15: 623–631.

Tiwari, P.B., Chapagain, P.P., and Üren, A. (2018). Investigating molecular interactions between oxidized neuroglobin and cytochrome c. Sci. Rep. 8: 10557.

Tubbs, J.L., Pegg, A.E., and Tainer, J.A. (2007). DNA binding, nucleotide flipping, and the helix-turn-helix motif in base repair by O^6-

alkylguanine-DNA alkyltransferase and its implications for cancer chemotherapy. DNA Repair 6: 1100–1115.

Warren, J.J., Forsberg, L.J., and Beese, L.S. (2006). The structural basis for the mutagenicity of O^6-methyl-guanine lesions. Proc. Natl. Acad. Sci. U. S. A. 103: 19701–19706.

Zak, P., Kleibl, K., and Laval, F. (1994). Repair of O^6-methylguanine and O^4-methylthymine by the human and rat O^6-methylguanine-DNA methyltransferases. J. Biol. Chem. 269: 730–733.

Zang, H., Fang, Q., Pegg, A.E., and Guengerich, F.P. (2005). Kinetic analysis of steps in the repair of damaged DNA by human O^6-alkylguanine-DNA alkyltransferase. J. Biol. Chem. 280: 30873–30881.

Supplementary Material: The online version of this article offers supplementary material (https://doi.org/10.1515/hsz-2021-0198).